



**Repositorio Institucional de la Universidad Autónoma de Madrid**

<https://repositorio.uam.es>

Esta es la **versión de autor** del artículo publicado en:

This is an **author produced version** of a paper published in:

Carbon 131 (2018): 229-237

**DOI:** <https://doi.org/10.1016/j.carbon.2018.01.104>

**Copyright:** © 2018 Elsevier Ltd

El acceso a la versión del editor puede requerir la suscripción del recurso

Access to the published version may require subscription

# Magnetic Anisotropy of Functionalized Multi-Walled Carbon Nanotube Suspensions

*Daniel Calle<sup>1,‡,¥</sup>, Viviana Negri<sup>1,2,‡</sup>, Carmen Munuera<sup>3</sup>, Luis Mateos<sup>4,‡</sup>, Isabel Lado Touriño<sup>5</sup>,  
Piedad Ros Viñegla<sup>5</sup>, Mariola O Ramírez<sup>4</sup>, Mar García-Hernández<sup>3</sup>, Sebastián Cerdán<sup>1\*,‡</sup> and  
Paloma Ballesteros<sup>2,‡</sup>*

<sup>1</sup>Instituto de Investigaciones Biomédicas “Alberto Sols”, CSIC-UAM, C/ Arturo Duperier 4, 28029, Madrid, Spain, <sup>2</sup>Laboratorio de Síntesis Orgánica e Imagen Molecular por Resonancia Magnética, Facultad de Ciencias, UNED, Unidad Asociada al CSIC, c/ Paseo Senda del Rey 9, 28040, Madrid, Spain, <sup>3</sup>Instituto de Ciencia de Materiales de Madrid, CSIC, C/ Sor Juana Inés de la Cruz 3, 28049, Cantoblanco, Madrid, Spain, <sup>4</sup>Dpto. Física de Materiales and Instituto Nicolás Cabrera, Universidad Autónoma de Madrid, 28049 Madrid, Spain, <sup>5</sup>Universidad Europea Madrid, C/ Tajo s/n, Villaviciosa de Odón, 28670, Madrid, Spain. ‡ Contributed equally.

KEYWORDS: Functionalized Multi-Walled Carbon Nanotubes, Aminopyrene, Magnetic Anisotropy, SQUID, Optical properties.

\* Corresponding Author. Phone: +34-91-585-4444, E-mail: [scerdan@iib.uam.es](mailto:scerdan@iib.uam.es) (Sebastián Cerdán)

19 ABSTRACT: We report on the magnetic properties of stable suspensions from oxidized  
20 Multiwalled Carbon Nanotubes (MWCNT) functionalized with aminopyrene (AP). MWCNT form  
21  $\pi$ - $\pi$  stacking adducts with AP (AP-MWCNT), originating homogenous, stable, suspensions in  
22 *N,N*-dimethylformamide (DMF) or melted agarose. First, we investigated the magneto-optical  
23 properties of these adducts. When applying series of pulsed magnetic fields to nanotube  
24 suspensions in DMF, the pattern of light dispersed increased during the magnetic pulse and  
25 decreased in the intervals, a behavior consistent with magnetic field induced orientation of the  
26 adducts. When adducts were suspended in a melted agarose gel under an external magnetic field,  
27 the extinction coefficient of polarized light through the gel, was larger when the polarization plane  
28 was parallel to the magnetic field direction. Based on the magneto-optical responses observed, we  
29 further investigated the magnetic properties of AP-MWCNT implementing Superconducting  
30 Quantum Interference Device (SQUID), Zero Field Cooling (ZFC) and Field Cooling (FC), and  
31 Thermogravimetric (TGA) and Differential Scanning Calorimetry (DSC) measurements. Pre-  
32 oriented AP-MWCNT suspensions depicted a clear superparamagnetic character with hysteresis  
33 loops revealing larger magnetic susceptibility values along their longitudinal axis. ZFC, FC and  
34 TGA/DSC revealed that these magnetic properties were preserved after thermal removal of  
35 aminopyrene from the AP-MWCNT adduct, suggesting that the nanotubular structure dominates  
36 the magnetic contributions. In summary, magneto-optical and SQUID measurements revealed that  
37 nanotube adducts in suspension, behave as nanoscale compass needles aligning their long axis  
38 parallel to externally applied magnetic fields.

## 1. Introduction

Carbon Nanotubes (CNT) have reached considerable interest in Physics, Chemistry and Biomedicine due to their outstanding physicochemical properties of electrical conductance, magnetic character, optical activity, thermal capacity, elasticity and chemical versatility.[1-8] These properties are thought to arise from their unique graphene structure as organized in a nanotubular arrangement, in which the asymmetric molecular organization determines their anisotropic properties.[9-11]

The magnetic properties of carbon nanotubes entail considerable relevance, since amorphous graphite is known to be non-magnetic,[12] while carbon nanotubes depict non zero magnetic moments.[11, 13] Indeed, a number of previous studies have addressed the magnetism of carbon nanotubes, either theoretically or experimentally, with different results.[5, 11, 13-20] Some authors reported that CNT present an inherent diamagnetic nature,[13-15] attributing the paramagnetic behavior to the metallic impurities.[16] In contrast, others described an intrinsic paramagnetic behavior of CNT due to the Aharonov-Bohm effect[5, 11, 17, 18] with magnetic susceptibility depending on their chirality, as metallic or semiconducting.[11, 19] Reasons for these discrepancies may involve the different characteristics of CNT preparations used; individual nanotubes[11] oriented in polymer films[13, 14] or co-suspended with DNA or in micelles.[19, 20] In addition, we and others reported previously, the alignment of nanotube suspensions in the magnetic fields normally used in Magnetic Resonance Imaging,[21, 22] a circumstance that could enable new applications in the field of contrast agents for biomedical imaging. However, a major difficulty limiting the investigation of the magnetic properties of carbon nanotubes has been to obtain, well characterized, stable suspensions of CNT enabling sufficiently prolonged and reproducible studies under homogeneous conditions.

We report here on the preparation and characterization of aminopyrene-MWCNT (AP-MWCNT) adducts suspended in *N,N*-dimethylformamide (DMF) solvent or melted agarose, two systems yielding stable, reproducible and homogeneous suspensions of AP-MWCNT adducts, allowing for the detailed investigation of the magnetic behavior of MWCNT. We obtained then magneto-optical measurements of light dispersion and absorption, complemented with Superconducting Quantum Interference Device (SQUID), Field Cooling (FC) and Zero Field Cooling (ZFC), and Thermogravimetric (TGA)/Differential Scanning Calorimetry (DSC) measurements to investigate the inherent superparamagnetic behavior of the suspensions and its anisotropy.

## 2. Experimental

### 2.1 Synthesis and characterization of $\pi$ - $\pi$ stacking adducts (AP-MWCNT)

The preparation of  $\pi$ - $\pi$  stacking adducts (Figure 1) proceeded in two steps: MWCNT oxidation and adduct formation.

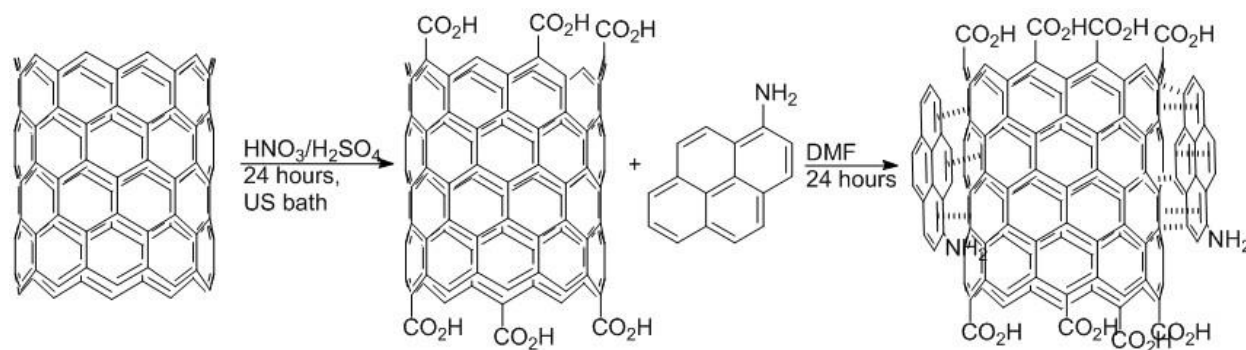


**Figure 1.** Synthesis of  $\pi$ - $\pi$  stacking adducts from MWCNT and aminopyrene (AP-MWCNT).

#### 2.1.1 MWCNT oxidation

Pristine MWCNT (300 mg) (Short-Purified, > 95 % carbon purity, < 2 % amorphous carbon, average diameter/length <10 nm/ 1-2  $\mu$ m, produced by chemical vapor deposition (CVD), purchased from Ses Research, Houston, Texas, US) were suspended in 36 mL of sulfuric (98

82 %)/nitric (65 %) acid mixture (3:1 v/v) and sonicated (24 h) in a water bath at room  
83 temperature[23-25]. Milli-Q water was then carefully added until pH of the suspension reached  
84 pH=3.0 (Universal Indicator paper pH1-pH14, Johnson Test Paper, Oldbury, UK) and the  
85 suspension was membrane filtered (0.45  $\mu\text{m}$ , Omnipore<sup>®</sup>PTFE, Madrid, Spain). The MWCNT  
86 filtrate was washed until eluate pH became neutral, and the resulting oxidized MWCNT dried at  
87 80 °C under vacuum (86 % yield). This treatment oxidized the CNT tips to carboxylic groups  
88 (MWCNTCOOH).[23-25] The oxidized MWCNT depicted the following properties: TXRF/ Fe:  
89 0.031 %, Co: 0.183 %, Ni: 0.007 %; FT-IR (ATR Ge),  $\nu$ : 3300, 1910, 1712, 1694, 1560, 1377,  
90 1152, 847  $\text{cm}^{-1}$  (Figure 3, blue).

#### 91 2.1.2 Adduct formation

92 MWCNTCOOH (25 mg) were sonicated in 65 mL of *N,N*-dimethylformamide (DMF) at 25 °C  
93 during 24 hours and 160 mg of 1-aminopyrene (AP) was added until a homogenous suspension  
94 was obtained.[26] The reaction was stirred in an ultrasonic bath (Fisher Scientific, Madrid, Spain)  
95 at room temperature for 24 hours. After solvent evaporation *in vacuo*, the resulting nanotubes were  
96 washed with diethyl ether (30 mL x 10 times) and filtered (Omnipore<sup>®</sup> membrane filtration, 0.45  
97  $\mu\text{m}$ ) until complete free AP removal, as detected by HPLC-MS. Finally the AP-MWCNT adducts  
98 were dried *in vacuo* at 60 °C for 24 hours (metal concentration was detected by TXRF, Fe: 0.046  
99 %, Co: 0.322 % and Ni: 0.005 %; FT-IR (ATR-Ge),  $\nu$  = 3407, 3238, 1907, 1715, 1572, 1413,  
100 1151, 1089  $\text{cm}^{-1}$ ).

101 After purification and removal of aminopyrene excess, Fourier Transform Infrared Spectroscopy  
102 (FT-IR), thermogravimetric analysis (TGA), and X-Ray Photoelectron spectroscopy (XPS)  
103 confirmed experimentally the functionalization, while Molecular Modeling simulations showed

that the aminopyrene molecules couples to the nanotube surface through  $\pi$ - $\pi$  stacking, adopting a parallel-displaced configuration (Supplementary Material Fig S2).

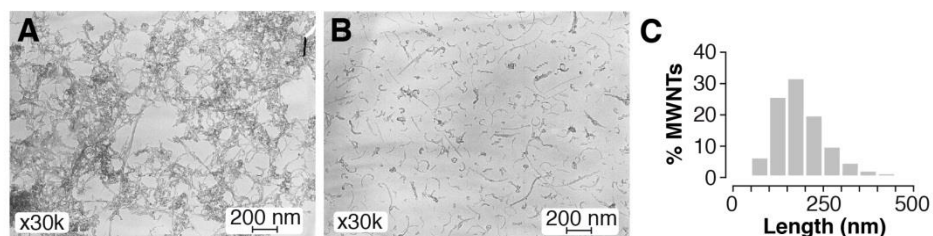


**Figure 2.** TEM images (200 kV) of commercial MWCNT (A), AP-MWCNT (B) and distribution length histogram (C). This chemical process results in a relatively homogenous distribution of nanotubes sizes with average lengths 170 nm.

The oxidation and adduct formation processes, resulted in length distributions of 75 - 250 nm (maximum around 170 nm), representing 91 % of sample lengths (Fig. 2C). This reduced significantly the bundles and entanglements of commercial MWCNT (Fig. 2A), favoring further homogenous suspensions in *N,N*-dimethylformamide (DMF) or in aqueous agarose gels.

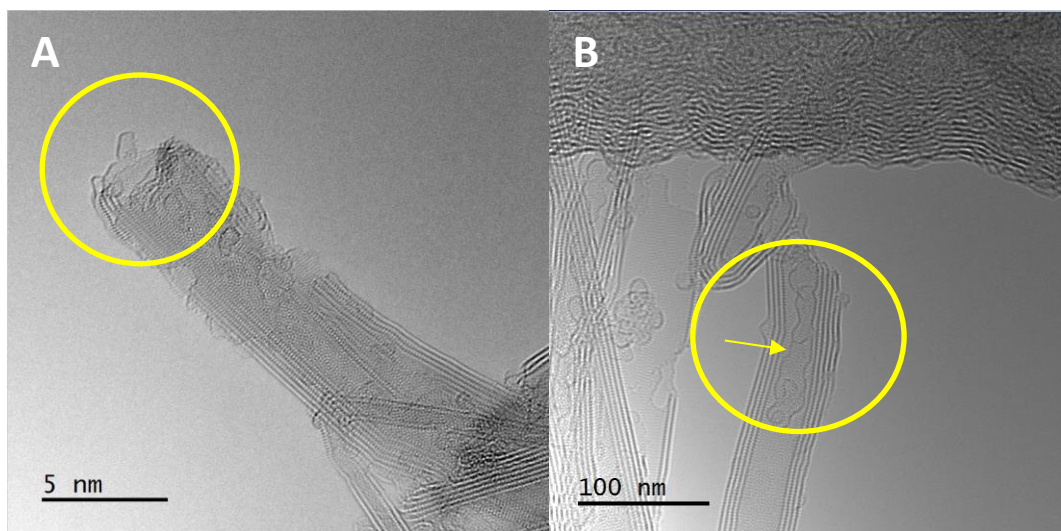


**Figure 3.** TEM images of oxidized MWCNT (A) and AP-MWCNT adducts (B) showing open ends and AP adsorption. Images acquired with a GRANDARM300cFEG microscope with corrective aberration in the objective lens.

Further TEM analyses (Figure 3), showed clearly the multiwalled carbon nanotube structure with open ends (yellow circles) as well as the AP molecules adsorbed on their surface in AP-MWCNTs adducts (yellow circle and arrow in 3B).

### 2.1.3 Fourier Transform Infrared Spectroscopy (FTIR)

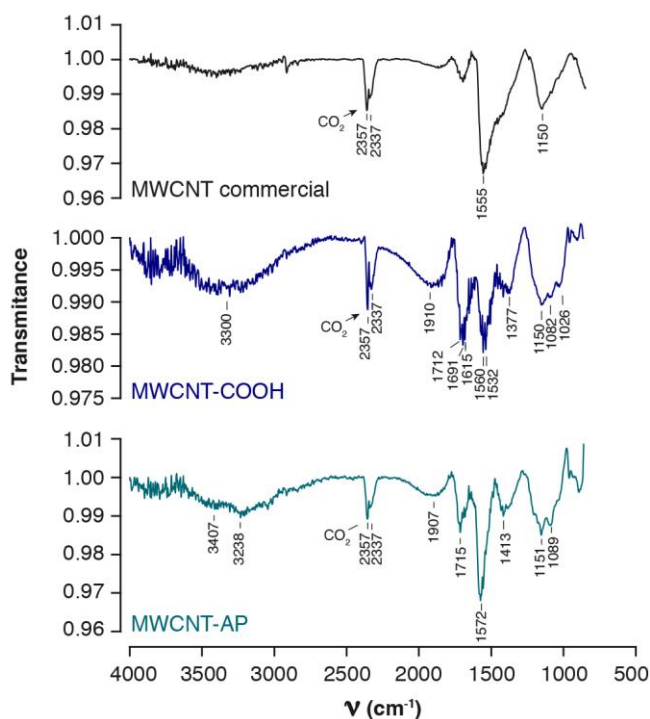


**Figure 3.** FTIR ATR (Ge) spectra of MWCNT (black), MWCNTCOOH (blue) and AP-MWCNT (green).

FTIR spectra (Figure 3) show progressive functionalization. Pristine MWCNT (black) present an intense peak at  $1555\text{ cm}^{-1}$ , from double bonds  $\nu\text{ C}=\text{C}$ , and bands from  $1200\text{ cm}^{-1}$  to  $800\text{ cm}^{-1}$ , derived from the MWCNT scaffolds. MWCNT-COOH (blue) display bands at  $3300\text{ cm}^{-1}$  from O-H stretching, at  $1712\text{ cm}^{-1}$  from C=O stretching, at  $1560\text{ cm}^{-1}$  from C=C stretching, and at  $1377\text{ cm}^{-1}$  C-O stretching, respectively. FT-IR spectra of AP-MWCNT (green) show, in addition to the



peaks present in the oxidized nanotubes, bands of N-H stretching at  $3400\text{ cm}^{-1}$  (overlapping with the bands of O-H stretching from carboxylic groups) and bands of C-N stretching at  $1151\text{ cm}^{-1}$ .

#### 2.1.4 Thermogravimetric Analysis (TGA)

We implemented thermogravimetric measurements to compare the degree of functionalization of MWCNT, MWCNT-COOH and AP-MWCNT.

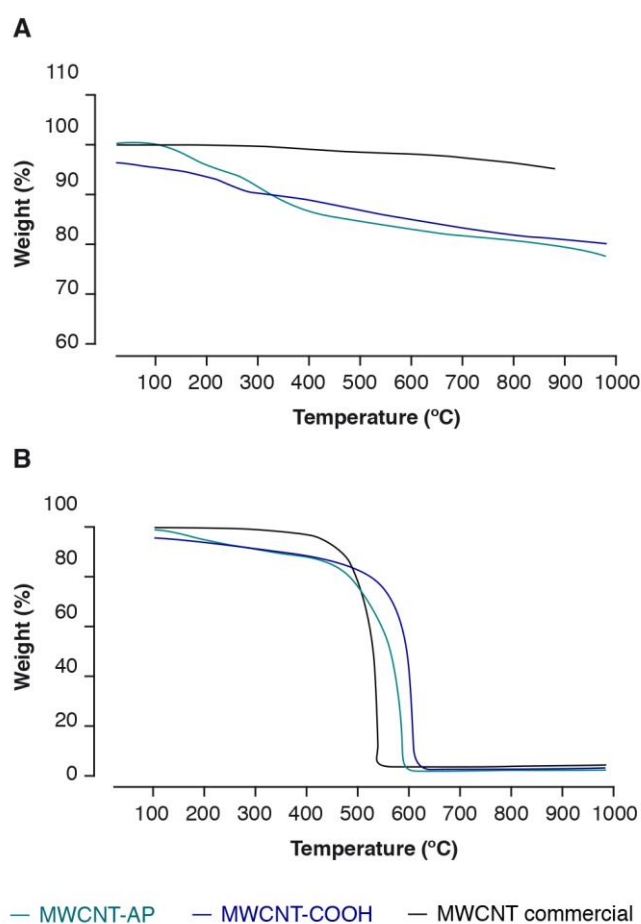


**Figure 4.** TGA analysis of MWCNT (black), oxidized MWCNT (blue) and  $\pi$ - $\pi$  stacking adducts AP-MWCNT (green) in Ar (A) or in Air (B).

To this end, TGA was performed under two different atmospheres; Ar, to investigate purity of starting materials and nanotube functionalization (Figure 4A); and air, to observe both

functionalization and the oxidized carbon of nanotubes (Figure 4B). TGA in Ar of MWCNT (black) shows only very moderate weight losses, confirming a high purity of the pristine material (Figure 4A). MWCNT-COOH (blue) and AP-MWCNT (green) originate in both cases, lower residues than pristine material, indicating a higher degree of functionalization (19.2 % in the oxidized nanotubes and 22.4 % in  $\pi$ - $\pi$  stacking adducts).

TGA in Air (Figure 4B) of pristine MWCNT (black) shows only weight losses close to 500-550 °C, corresponding to carbon nanotubes. MWCNT-COOH (blue) displays larger weight losses than MWCNT. The first weight loss (10.3 %), between 90 and 350 °C, is due to CO<sub>2</sub> moieties, while the second (86,62 %), between 400 to 600 °C, is due to the carbons of CNT, resulting in a final residue of 3.08 %. Finally, AP-MWCNT (green) show weight losses of; 4.9 % between 100-220 °C, 9.3 % between 220 and 400 °C, and 83,43% from 450 to 600 °C, resulting in a final residue of 2.37 % at 980 °C. These transitions correspond primarily, for increasing temperatures, to the weight losses derived from aminopyrene, CO<sub>2</sub> moieties and carbon from the MWCNT, respectively.

### 2.1.5 X Ray Photoelectron Spectroscopy (XPS)

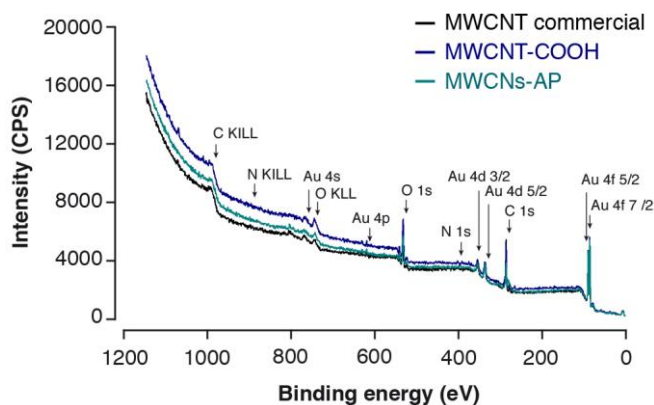


**Figure 5.** XPS analysis of MWCNT (black), oxidized MWCNT (blue) and  $\pi$ - $\pi$  stacking adduct AP-MWCNT (green).

XPS analysis (Figure 5) shows the atomic species present in the surfaces of MWCNT (black), oxidized MWCNT (blue) and AP-MWCNT (green). In MWCNT-COOH, the O/C ratio (0.339) increases when compared to pristine MWCNT (0.27), due to the carboxylic groups introduced in the oxidation process. An important increment in the N/C ratio (0.092) was found in AP-MWCNT as compared to pristine and oxidized MWCNT (0.014). In summary, O/C and N/C ratios in the three samples illustrated the oxygen and nitrogen increments in oxidized MWCNT and  $\pi$ - $\pi$  stacking adducts.

### 3. Results and discussion

We first investigated the magnetic behavior of AP-MWCNT suspensions in an external magnetic field using different magneto-optical approaches. First, we studied the response of AP-MWCNT suspensions (DMF, 3 mg/mL) using a QuantaMaster spectrofluorimeter (PTI, Birmingham, NJ, USA) measuring light dispersion and sample anisotropy (510 nm). To induce an external magnetic field inside the optical chamber, we implemented a home-made device consisting in an electromagnet (50 Gauss,  $5 \cdot 10^{-3}$  T) whose magnetic field was perpendicular to the illuminating beam and the detector. The device allowed switching transiently the magnetic field between the “off” and “on” positions, making it possible to measure the magnetic field dependence of the light dispersed by the AP-MWCNT suspension. Figure 6A clearly shows how the presence of the magnetic field (“on”), induced a significant increase in light dispersion in the plane perpendicular to the magnetic field. These results suggest an induced orientation of the AP-MWCNT adducts parallel to the applied magnetic field (Fig 6B-C).

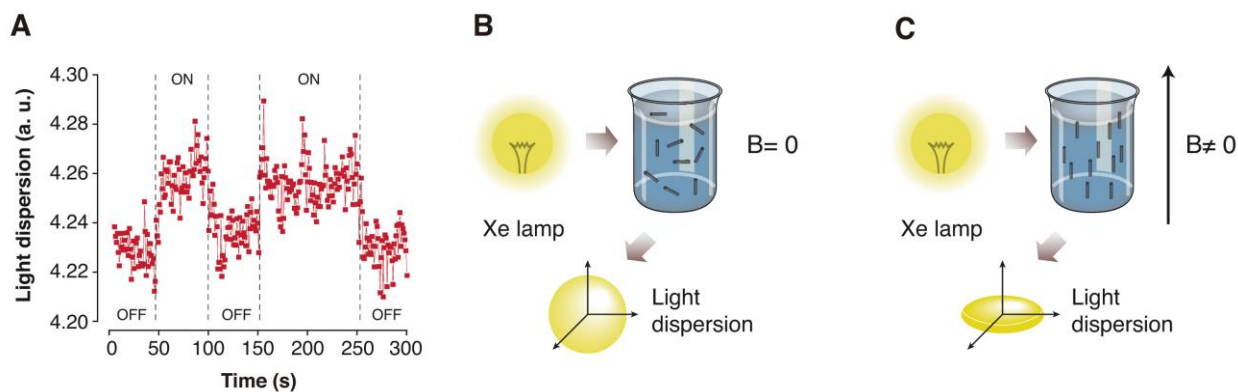


**Figure 6.** A: Light dispersion as a function of time while the magnetic field is switched “on” and “off”. B, C: Schematic diagram of light dispersion with ( $B \neq 0$ ) and without ( $B = 0$ ) the presence of an external the magnetic field.

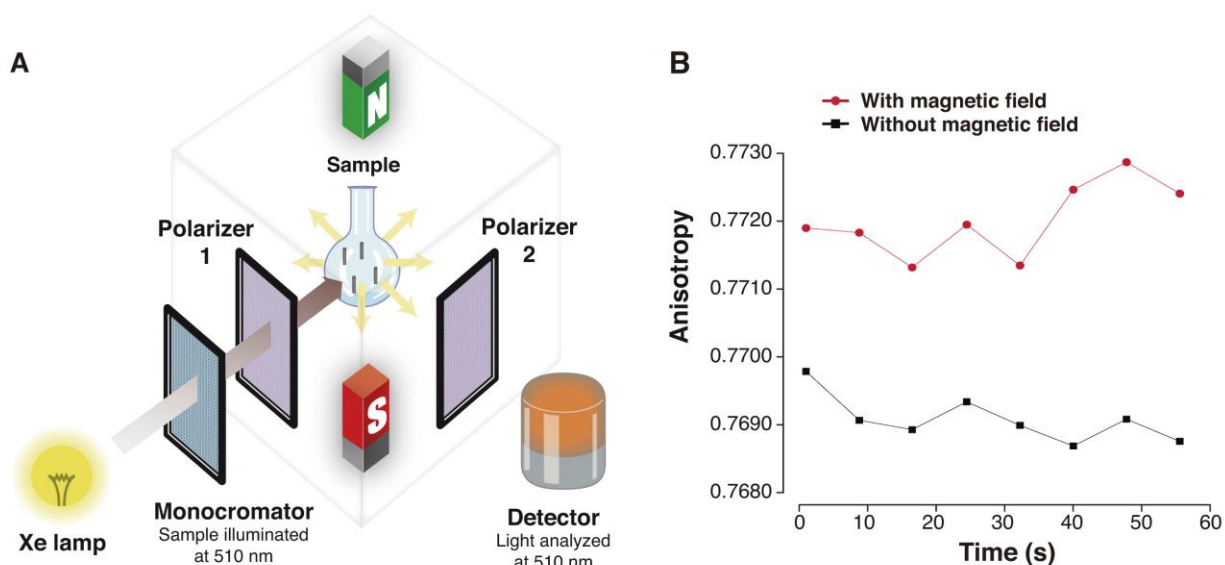


**Figure 7.** A: Dispersed light is collected at  $90^\circ$  of the incident beam with a coplanar detector to calculate the anisotropy of the sample. B: Anisotropy of the light dispersion in the presence and absence of magnetic field.

We completed the measurements of light dispersion with steady-state optical anisotropy measurements (Supplementary Material Eq. 1) with the same set-up but using polarized light (510 nm) illumination (Fig. 7A). Optical anisotropy was measured at steady state either, in the presence (“on”) or in the absence (“off”) of applied magnetic field (Fig. 7B). Optical anisotropy became

larger in the presence of the applied magnetic field, a finding consistent with a preferential orientation of the AP-MWCNT adducts in the direction of the applied magnetic field. Note that optical anisotropy is significantly smaller in the case of the randomly distributed AP-MWCNT suspensions in the absence of magnetic field.

To further explore the optical anisotropy of AP-MWCNT, we measured the optical absorption of the suspension under polarized light. The experiments were performed using a spectrophotometer (LAMDA 1050 UV/Vis/NIR, PerkinElmer, Waltham, MA, USA) at 340 nm, which corresponds to one of the main absorption peaks of aminopyrene.[27, 28] Aminopyrene presents remarkable absorption anisotropy depending on the orientation of the aromatic ring with respect the polarization plane of the illuminating light beam. In particular, the absorption peak at 340 nm originates when the long axis of the aminopyrene ring is positioned parallel to the light polarization plane. Therefore, this property can be used to investigate the orientation of AP-MWCNT adducts, since aminopyrene is coupled to the nanotube with its long axis oriented parallel to the long nanotube axis (Supplementary Information Fig S2).[29] On this basis, increased absorption at 340 nm reveals an increased proportion of AP-MWCNT oriented parallel to the light polarization plane.

Using this strategy, we investigated anisotropy in the absorption of polarized light in two different preparations, i) AP-MWCNT suspended in DMF (3 mg/mL), and ii) AP-MWCNT pre-oriented magnetically in a melted agarose (0.5 %) gel (Supplementary Material/Light absorption). Under the latter conditions, AP-MWCNT adducts maintained the orientation induced magnetically during solidification of the agarose gel to room temperature. First, we measured the absorption of the nanotubes in suspension, using the same home-made magnet previously adapted to the spectrofluorometer in the experiment described in Figure 7A.

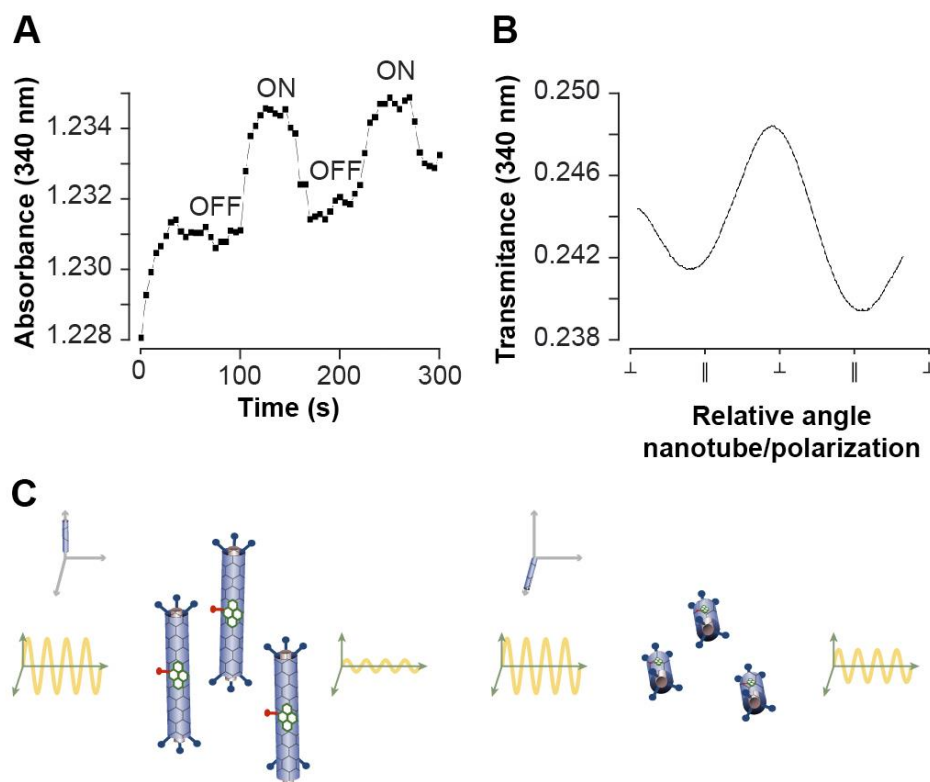


**Figure 8.** A: Polarized light absorbance is higher in AP-MWCNT suspensions when the magnetic field is switched on parallel to the light polarization plane. B: A cosine function behaviour of the transmittance at 340 nm is observed when the polarizer rotates the polarization plane of the illuminating light with respect to an immobile solid block of agarose gel with pre-oriented AP-MWCNT. The transmittance reaches maximum values (and absorption minimal values) when nanotubes are perpendicular to the light polarization plane. C: The absorption of polarized light is higher when the AP-MWCNT are oriented parallel to the light polarization plane, because of the anisotropic absorption of the aminopyrene ring.

The sample was then illuminated with linear polarized light at 340 nm, oriented along the magnetic field direction. Figure 8A shows the variations in the absorbance of the polarized light while the magnetic field is switched “on” and “off” sequentially. Clearly, the suspension exhibits a higher absorbance when the magnetic field is turned “on”, indicating an increased proportion of AP-MWCNT oriented parallel to the external magnetic field applied (Figure 8C).

Finally, the AP-MWCNT were pre-aligned magnetically and fixed in a known direction in a solid agarose gel. To this end, AP-MWCNT were suspended in a melted agarose gel (60 °C), inside a 7 Tesla magnet (Bruker Pharmascan, 16 cm bore), while letting the suspension cool down to room temperature (22 °C), thus trapping the nanotubes within the solid agarose gel with the orientation acquired magnetically before cooling. We accommodated then the gel containing pre-oriented AP-MWCNT within the optical path of the polarized light spectrophotometer and measured the transmittance of the suspension as a function of the relative rotation angle of the linear polarizer with respect to the pre-oriented AP-MWCNT gel (Figure 8B). The transmittance shows a maximum when the polarization of the light is perpendicular to the AP-MWCNT orientation ( $\perp$ ) (Figure 8C), while it reaches a minimum when is parallel ( $\parallel$ ), reproducing this behaviour periodically when the polarizer rotates progressively. In summary, the rotation of the polarizer caused a periodical behaviour in the absorption of the polarized light as expected from an oriented AP-MWCNT suspension.

In conclusion, magneto-optical results obtained with AP-MWCNT in suspension (Figure 8A) or fixed in agarose gels (Figure 8B) demonstrate; (i) increased light absorption when the external magnetic field is applied in DMF suspensions, and (ii) increased polarized light absorption when AP-MWCNT are pre-oriented in melted agarose gels parallel to the field (Figure 8C). These findings are consistent with a magnetic field dependent orientation of the AP- MWCNT adducts both in DMF suspensions and in melted agarose gels.

Considering these findings, we addressed the intrinsic magnetic properties of AP-MWCNT using a Superconducting Quantum Interference Device (SQUID). Briefly; we obtained magnetic loops from a suspension of AP-MWCNT (1mg/mL) in DMF, pre-oriented at room temperature (300 K) in an external magnetic field (0.5 T) perpendicular to the SQUID measuring field. The

suspension was then frozen to 5 K (DMF solidifies at 212.15 K), maintaining in this way the pre-orientation of the entrapped AP-MWCNT. Then, we placed the frozen sample in the SQUID cavity and measured the hysteresis loop at 5 K (“perpendicular” configuration). Right after, the temperature was increased to 300 K, melting the suspension and reorienting it, this time in the SQUID measuring field direction, and cooling down again to 5 K within an applied field of 0.5 T. A second hysteresis loop was then measured in which the AP-MWCNT were aligned in the direction of the field (“parallel” configuration).

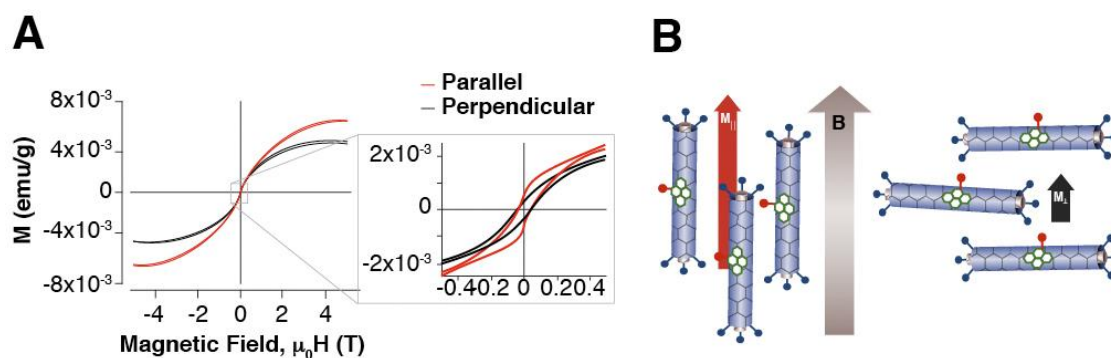


**Figure 9.** Magnetic hysteresis loops (A) of AP-MWCNT oriented parallel (red) or perpendicular (black) to the magnetic field of SQUID. The inset shows an expanded view of the low field region. The magnetization of the nanotubes is higher in the parallel orientation than in the perpendicular (B).

Figure 9A shows both hysteresis loops, where the red and black lines correspond to the parallel and perpendicular orientations, respectively. Clear differences become detectable when both cycles are compared, expanded in more detail in the inset corresponding to the low-field region. As expected, the parallel configuration showed higher values of the saturation magnetization than the perpendicular configuration, therefore exhibiting a clear anisotropic behavior (Fig. 9B). The alignment of the magnetic moments of the AP-MWCNT adducts in the direction of the measuring applied field is clearly more efficient when the AP-MWCNT have been cooled down with an applied field in the same direction (parallel), rendering higher saturated values of the



magnetization and larger remanence. However, it should be noted here that the shape of the isotherms cycles (S shaped), in the parallel and perpendicular configurations, could point out to the existence of an additional contribution to the ferromagnetic one causing the finite remanence and coercivity. This contribution could be related to a disordered spin glass-like behavior of highly frustrated moments that could be responsible for the irreversibilities observed at high fields in the hysteresis cycles.

The same protocol was followed in a sample containing only the DMF solvent (Supplementary Material Fig S1), to discard any influence of the solvent on the magnetic differences observed in Figure 9A. Only the diamagnetic contribution was observed, with no measurable difference in the magnetic properties depending on the orientation of the aligning field. This proves that the differences observed in Figure 9A are due to the different orientations of the nanotube adducts with respect to the measuring field, as induced by the pre-alignment field as described above. Note that in the data shown in Figure 9A the corresponding diamagnetic contributions have been subtracted.

We investigated further the origin of the superparamagnetic behavior by assessing the relative contributions of the aminopyrene molecules and the MWCNT structure. Figure 10A shows magnetic hysteresis loops measured at 5K for the raw MWCNT used as starting material, the nanotubes obtained after the oxidation process (MWCNT-COOH) and the amino-pyrene adducts (AP-MWCNT), measured in powder form. The inset shows the complete cycle,  $\pm 5T$ , in which saturation is almost reached for the MWCNT sample but not for MWCNT-COOH or AP-MWCNT. This could be related to the existence of hard spins that find it difficult to completely align with the field due to magnetic disorder and frustration. The main graph of Figure 10A shows

an expanded view of the low field region, where clear differences are observed between the three samples.

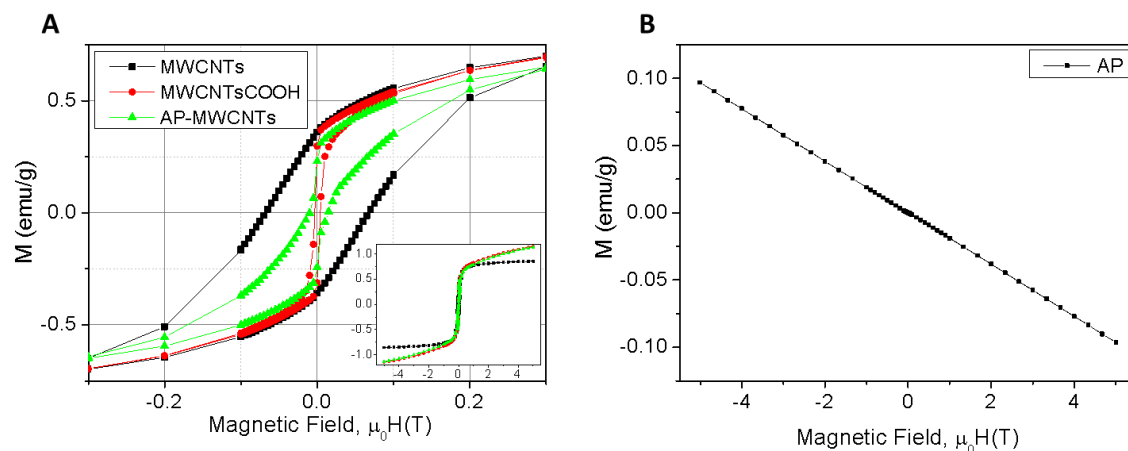
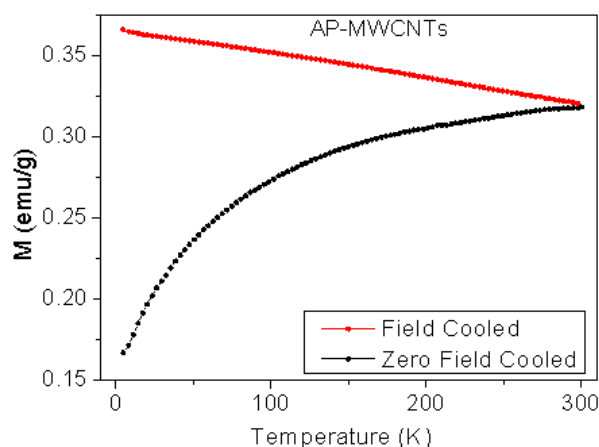


Figure 10. A: Magnetic hysteresis loops measured at 5K of raw MWCNT (black squares), MWCNT-COOH (red circles) and AP-MWCNT (green triangles). The inset shows the complete cycle whereas an expanded view of the low field region is presented in the main panel. The corresponding diamagnetic contribution has been subtracted. (B) Magnetic hysteresis loop of amynopyrene (AP).

Raw MWCNT show a ferromagnetic response with a coercive field of 650 Oe. After the oxidation procedure, this ferromagnetic behavior is lost, most probably due to the removal of the metal impurities detected by TXRF in the resulting MWCNT-COOH preparation as compared to the raw MWCNT (MWCNT-COOH/raw; % Fe 0.031/0.159, % Co 0.183/0.611 y % Ni 0.007/0.014). For MWCNT-COOH, the main magnetic component is a ferromagnetic signal, while for AP-MWCNT is the sum of two contributions. The first one is narrow and related to that observed in MWCNT-COOH; the second one exhibits “wasp waist” shape, related to some kind of directional order gained through the AP-MWCNT interaction. By directional order, we mean a preferred orientation of the axis of the elemental units (the adduct, in our case).<sup>1</sup>

Figure 10B shows the magnetic hysteresis loop of aminopyrene (AP) measured at 5K, where only a diamagnetic contribution is observed. Consequently, aminopyrene by itself is not responsible for the observed magnetism in the AP-MWCNT adduct.

We also explored the M-T curves, as suggested. Zero field cooled (ZFC) and field cooled (FC) temperature dependent magnetization for the AP-MWCNT adducts are shown in Figure 11. We observed large irreversibility between FC and ZFC temperature dependent magnetizations, as measured in an applied field of 500 Oe. This is related to the existence of strong magnetic frustration in the system. Within the temperature range explored, no drop in magnetization is observed, indicating a Curie Temperature ( $T_c$ ) above room temperature. Similar ZFC-FC curves are obtained for the raw and oxidized MWCNT (Figure S2 Supplementary Material).



**Figure 11.** Zero field cooled (ZFC) and field-cooled (FC) evolution of the magnetization as a function of temperature for AP-MWCNT in powder form.

We pursued the determination of  $T_c$  at higher temperatures using TGA/DSC measurements (Figure S3, Supplementary Material). We determined TGA/DSC profiles in samples of Aminopyrene, raw MWCNTs used as starting material, oxidized MWCNT-COOH and AP-MWCNT. TGA /DSC of Aminopyrene revealed the thermal destruction of this molecule at 300

°C, while TGA/DSC of MWCNT, and MWCNT-COOH revealed that the nanotube structure was maintained up to much higher temperatures. Although we could not detect precisely  $T_c$  in these measurements, it is clearly much above the temperature of thermal destruction of AP, suggesting that the MWCNT structure and its magnetic properties are maintained at higher temperatures than that of AP desorption/destruction. Interestingly,  $T_c$  of helical carbon nanotubes has been reported to be even higher than 900 degrees (Zuang et al (2013) AIP Advances 3, 052112).<sup>2</sup>

Our evidence indicates that the superparamagnetic behavior of AP-MWCNT adducts is maintained after AP has been thermally destroyed/desorbed and thus, is mainly derived from the MWCNT structure.

To summarize, we investigated herein the magnetic properties of AP-MWCNT suspensions in DMF or agarose gels using a combination of magnetic and magneto-optical measurements. By collecting magneto-optical measurements, we showed that when an external magnetic field is applied to a suspension of AP-MWCNT these are oriented predominantly parallel to the direction of the external field. These findings prompted us to confirm the intrinsic magnetic anisotropy of AP-MWCNT using SQUID. Magnetic hysteresis loops demonstrated that AP-MWCNT preparations exhibit intrinsic magnetic anisotropy, with higher magnetizations achieved when the nanotubes are oriented parallel to the magnetic field. FC, ZFC and TGA/DSC measurements indicate that the superparamagnetic behavior is not derived from the AP molecule itself and therefore derived from the nanotubular structure and the  $\pi$ - $\pi$  interaction with adsorbed AP.

Taken together, our results show that AP-MWCNT in suspension behave as nanoscale compass needles, a circumstance that can be further exploited in multiple fields including biomedical imaging; as directional contrast agents, or in optics; as moldable polarizers by adding optically active molecules to absorb/emit light of different wavelengths in an orientation dependent manner.

353

354 ASSOCIATED CONTENT

355 **Supplementary Material.** Supplementary material to this article can be found, free of charge, at  
356 (<http://...>).

357 AUTHOR INFORMATION

358 **Corresponding Author**

359 \*Sebastián Cerdán. Instituto de Investigaciones Biomédicas “Alberto Sols”, C/ Arturo Duperier  
360 4, Madrid, 29029, Spain, phone: +34-91-585-4444, FAX: +34-91-585-4401, email:  
361 [scerdan@iib.uam.es](mailto:scerdan@iib.uam.es).

362 ORCID: [0000-0001-9965-0270](https://orcid.org/0000-0001-9965-0270)

363 **Present Addresses**

364 †Luis Mateos. Optoelectronics Research Centre, University of Southampton, Southampton SO17  
365 1BJ, UK.

366 ‡Daniel Calle, Laboratorio de Imagen Médica, Hospital Universitario Gregorio Marañón, c/ Dr.  
367 Esquerdo 56, 28007, Madrid (Spain).

368 **Author Contributions**

369 DC‡ and VN‡ prepared and oriented the AP-MWCNT suspensions and implemented the magneto-  
370 optical devices and measurements, writing the first draft. CM and MG performed and interpreted  
371 the SQUID approach. LM, MR and PR implemented and interpreted the polarized  
372 spectrophotometer measurements. IL performed the molecular modelling simulations. SC‡ and

PB‡ conceived the experiments and wrote the final draft with all authors commenting. ‡Authors contributed equally to this work.

### **Conflict of Interest Disclosure**

The authors declare no competing financial interest.

### **Funding Sources**

This work was supported in part by grants SAF2014-53739-R/ IPT-2012-06000 (to SC), CTQ-2013-47669-R (to PB) and MAT2013-43301-R and MAT2016-76106-R (to M O Ramírez) from the Spanish Ministry of Economy and Competitiveness and grants S2010/BMD-2349 (to PB and SC) and S2013/MIT-2740 (to M O Ramírez) from the Community of Madrid. DC and VN held postdoctoral contracts from CSIC. CM acknowledges the financial support by the “Ramón y Cajal” Program of MINECO (RYC-2014-16626).

### **Notes**

The authors declare no competing financial interest.

### **ACKNOWLEDGMENT**

Authors wish to express their gratitude to Mr. Javier Pérez, CSIC, for professional drafting of the illustrations and dedicate this article to Prof. Paloma Ballesteros on her retirement.

### **ABBREVIATIONS**

AP-MWCNT, aminopyrene functionalized multiwalled carbon nanotubes; CNT, carbon nanotubes; DMF, *N,N*-dimethylformamide; DSC, Differential Scanning Calorimetry, FC, Field Cooling, MWCNT, multiwalled carbon nanotubes; MWCNT-COOH, oxidized multiwall carbon

395 nanotubes, SQUID, Superconducting quantum interference device; TGA, thermogravimetric  
396 analyses; XPS, X-ray photoelectron spectra, ZFC, zero field cooling

397

## 398 REFERENCES

- 399 [1] S. Iijima, Helical microtubules of graphitic carbon, *Nature* 354(6348) (1991) 56-58.  
400 doi:10.1038/354056a0
- 401 [2] M.J. O'connell, Carbon nanotubes: properties and applications, CRC press 2006. ISBN-  
402 13: 978-0849327483
- 403 [3] A. Jorio, G. Dresselhaus, M.S. Dresselhaus, Carbon nanotubes: advanced topics in the  
404 synthesis, structure, properties and applications, Springer 2008.
- 405 [4] T. Ebbesen, H. Lezec, H. Hiura, J. Bennett, H. Ghaemi, T. Thio, Electrical conductivity of  
406 individual carbon nanotubes, *Nature* 382(6586) (1996) 54-56. doi:10.1038/382054a0
- 407 [5] H. Ajiki, T. Ando, Aharonov-Bohm effect in carbon nanotubes, *Physica B: Condensed*  
408 *Matter* 201 (1994) 349-352. [https://doi.org/10.1016/0921-4526\(94\)91112-6](https://doi.org/10.1016/0921-4526(94)91112-6)
- 409 [6] M. Damnjanović, I. Milošević, T. Vuković, R. Sredanović, Full symmetry, optical activity,  
410 and potentials of single-wall and multiwall nanotubes, *Physical Review B* 60(4) (1999) 2728-  
411 2739. DOI: <https://doi.org/10.1103/PhysRevB.60.2728>
- 412 [7] S. Berber, Y.-K. Kwon, D. Tomanek, Unusually high thermal conductivity of carbon  
413 nanotubes, *Physical Review Letters* 84(20) (2000) 4613-4616  
414 DOI: <https://doi.org/10.1103/PhysRevLett.84.4613>
- 415 [8] S. Iijima, C. Brabec, A. Maiti, J. Bernholc, Structural flexibility of carbon nanotubes, *The*  
416 *Journal of chemical physics* 104 (1996) 2089. doi: <http://dx.doi.org/10.1063/1.470966>
- 417 [9] R.S. Ruoff, D.C. Lorents, Mechanical and thermal properties of carbon nanotubes, *Carbon*  
418 33(7) (1995) 925-930. [https://doi.org/10.1016/0008-6223\(95\)00021-5](https://doi.org/10.1016/0008-6223(95)00021-5)
- 419 [10] J.P. Lu, Elastic Properties of Carbon Nanotubes and Nanoropes, *Physical Review Letters*  
420 79(7) (1997) 1297-1300. DOI: <https://doi.org/10.1103/PhysRevLett.79.1297>
- 421 [11] T. Searles, Y. Imanaka, T. Takamasu, H. Ajiki, J. Fagan, E. Hobbie, et al., Large anisotropy  
422 in the magnetic susceptibility of metallic carbon nanotubes, *Physical Review Letters* 105(1)  
423 (2010) 017403. DOI: <https://doi.org/10.1103/PhysRevLett.105.017403>
- 424 [12] T.L. Makarova, B. Sundqvist, R. Hohne, P. Esquinazi, Y. Kopelevich, P. Scharff, et al.,  
425 Magnetic carbon, *Nature* 413(6857) (2001) 716-8. DOI: <http://dx.doi.org/10.1038/35099527>
- 426 [13] F. Tsui, L. Jin, O. Zhou, Anisotropic magnetic susceptibility of multiwalled carbon  
427 nanotubes, *Applied Physics Letters* 76(11) (2000) 1452-1454. doi:  
428 <http://dx.doi.org/10.1063/1.126061>
- 429 [14] O. Chauvet, L. Forro, W. Bacsa, D. Ugarte, B. Doudin, W.A. de Heer, Magnetic  
430 anisotropies of aligned carbon nanotubes, *Physical review. B, Condensed matter* 52(10) (1995)  
431 R6963-R6966. DOI: <https://doi.org/10.1103/PhysRevB.52.R6963>
- 432 [15] A. Kotosonov, Texture and magnetic anisotropy of carbon nanotubes in cathode deposits  
433 obtained by the electric-arc method, *Journal of Experimental and Theoretical Physics Letters*  
434 70(7) (1999) 476-480. DOI: <https://doi.org/10.1134/1.568199>

- [16] K. Lipert, M. Ritschel, A. Leonhardt, Y. Krupskaya, B. Büchner, R. Klingeler, Magnetic properties of carbon nanotubes with and without catalyst, *Journal of Physics: Conference Series*, IOP Publishing, 2010, p. 072061. DOI <https://doi.org/10.1088/1742-6596/200/7/072061>
- [17] W. Tian, S. Datta, Aharonov-Bohm-type effect in graphene tubules: A Landauer approach, *Physical Review B* 49(7) (1994) 5097. DOI: <https://doi.org/10.1103/PhysRevB.49.5097>
- [18] S. Roche, G. Dresselhaus, M. Dresselhaus, R. Saito, Aharonov-Bohm spectral features and coherence lengths in carbon nanotubes, *Physical Review B* 62(23) (2000) 16092. DOI: <https://doi.org/10.1103/PhysRevB.62.16092>
- [19] S. Zaric, G.N. Ostojic, J. Kono, J. Shaver, V.C. Moore, R.H. Hauge, et al., Estimation of magnetic susceptibility anisotropy of carbon nanotubes using magnetophotoluminescence, *Nano Letters* 4(11) (2004) 2219-2221. DOI: 10.1021/nl0486012
- [20] O.N. Torrens, D.E. Milkie, H.Y. Ban, M. Zheng, G.B. Onoa, T.D. Gierke, et al., Measurement of chiral-dependent magnetic anisotropy in carbon nanotubes, *Journal of the American Chemical Society* 129(2) (2007) 252-3. DOI: 10.1021/ja066719+
- [21] V. Negri, A. Cerpa, P. Lopez-Larrubia, L. Nieto-Charques, S. Cerdan, P. Ballesteros, Nanotubular paramagnetic probes as contrast agents for magnetic resonance imaging based on the diffusion tensor, *Angewandte Chemie* 49(10) (2010) 1813-5. DOI: 10.1002/ange.200906415
- [22] A. Cerpa, M. Köber, D. Calle, V. Negri, J.M. Gavira, A. Hernanz, et al., Single-walled carbon nanotubes as anisotropic relaxation probes for magnetic resonance imaging, *MedChemComm* 4(4) (2013) 669-672. DOI: 10.1039/C3MD20235F
- [23] J. Liu, A.G. Rinzier, H. Dai, J.H. Hafner, R.K. Bradley, P.J. Boul, et al., Fullerene pipes, *Science* 280(5367) (1998) 1253-1256. DOI: 10.1126/science.280.5367.1253
- [24] S. Li, W. Wu, S. Campidelli, V. Sarnatskaia, M. Prato, A. Tridon, et al., Adsorption of carbon nanotubes on active carbon microparticles, *Carbon* 46(7) (2008) 1091-1095. <https://doi.org/10.1016/j.carbon.2008.03.010>
- [25] C. Samori, R. Sainz, C. Ménard-Moyon, F.M. Toma, E. Venturelli, P. Singh, et al., Potentiometric titration as a straightforward method to assess the number of functional groups on shortened carbon nanotubes, *Carbon* 48(9) (2010) 2447-2454. <https://doi.org/10.1016/j.carbon.2010.03.015>
- [26] S. Cosnier, M. Holzinger, Design of carbon nanotube-polymer frameworks by electropolymerization of SWCNT-pyrrole derivatives, *Electrochimica Acta* 53(11) (2008) 3948-3954. <https://doi.org/10.1016/j.electacta.2007.10.027>
- [27] F.D. Saeva, The optical properties of anisotropically ordered solutes in cholesteric liquid crystalline mesophases, *Pure and Applied Chemistry* 38(1-2) (1974) 25-36. DOI: <https://doi.org/10.1351/pac197438010025>
- [28] M. Vasak, M.R. Whipple, A. Berg, J. Michl, Magnetic circular dichroism of cyclic. pi.-electron systems. 13. Derivatives of pyrene, *Journal of the American Chemical Society* 100(22) (1978) 6872-6877. DOI: 10.1021/ja00490a013
- [29] P. Leyton, J.S. Gomez-Jeria, S. Sanchez-Cortes, C. Domingo, M. Campos-Vallette, Carbon nanotube bundles as molecular assemblies for the detection of polycyclic aromatic hydrocarbons: surface-enhanced resonance Raman spectroscopy and theoretical studies, *J Phys Chem B* 110(13) (2006) 6470-4. DOI: 10.1021/jp056379z